Available online at www.sciencedirect.com
SCIENCE DIRECT®
International Journal of Heat and Mass Transfer 47 (2004) 573–588
International Journal of HEAT and MASS TRANSFER
www.elsevier.com/locate/ijhmt

Application of a new finite integral transform method to the wave model of conduction

P. Duhamel *

Laboratoire de Thermique, CNAM, 75141 Paris Cedex 03, France

Received 7 January 1999; received in revised form 1 May 2003

Abstract

A new finite integral transform method [Int. J. Heat Mass Transfer 44 (2001) 3307] is applied to the wave model of conduction. It is compared with a standard method of solution of the hyperbolic conduction equation. The temperature fields coincide. The chosen test problem and its results bring to the foreground some of the difficulties of standard technique applications. These difficulties are by-passed when using the new method.

The Cattaneo Vernotte model is then tested through a comparison of its results with transient molecular dynamics simulations taken from Volz [Transferts de chaleur aux temps ultra-courts par la technique de la dynamique moléculaire, Thèse, Univ. de Poitiers, 1996]. When the used parameters of the continuous model are near their equilibrium values, the agreement remains weakly qualitative. An adaptation of these parameter values, notably the diffusion time scale, can give a quantitative coincidence; but never is the agreement obtained for both studied variables (internal energy and flux density). These observations are discussed. Various causes liable to justify the realized adaptations of parameters are considered. None of them gives a right explanation. Concerning the impossibility of making both variables coincide, the source of conflicts is as much in the constitutive law as in the energy conservation law. The key seems to be in thermodynamics.

1. Introduction

The aim of our previous paper [1] was to investigate a new finite integral transform (FIT) which suits the solving of linear systems of coupled partial derivative equations. When used within the framework of the Cattaneo-Vernotte model [2,3] the proposed transform leads to a method for solving hyperbolic thermal problems under less stringent hypotheses than was previously needed. Furthermore, it separates the variables in non-homogeneous media. This new method of solution is tested in the first part of this paper.

Of course the new method does not resolve the issue of the relevance of the Cattaneo–Vernotte (C–V) law [2,3] which, although sound from a physical standpoint, [1] even remains under suspicion. We list a few common criticisms:

- The use of the continuity hypothesis loses credibility when the medium consists of few atomic layers.
- Non-physical results such as over-or-under-shooting, [1] may appear.
- Other constitutive internal laws such as the dual phase-lag model of Tzou [4] yield good results [5], and are also credible candidates in a non-Fourier context.

The controversy is not over yet in view of the difficulties of performing conclusive experiments. The weakness of space and time scales where non-Fourier phenomena become relevant (see Ref. [6], for example) in homogeneous media, is the first well-known constraint. Pure initial and boundary conditions are difficult to control because of surrounding constraints; since a given internal constitutive model cannot be used without associated initial and boundary conditions and since, of course, these

* Tel.: +33-1-4027-2912; fax: +33-1-4940-6176.
E-mail address: duhamel@cnam.fr (P. Duhamel).

[1] See part 1 and part 2 of Ref. [1] for a more in depth analysis of the underlying physics.

0017-9310/$ - see front matter © 2003 Elsevier Ltd. All rights reserved.
doi:10.1016/S0017-9310(03)00385-5

Nomenclature

a'	thermal diffusivity
$\tilde{a}_k(t)$	transformed function (standard finite integral transform)
e	thickness
$E, E(t)$	internal energy
$H(\cdot)$	Heaviside's function
Kn_p	phonon Knudsen number ($Kn_p = \sqrt{3a'\tau'}/e' = \sqrt{3\tau}$)
$\hat{p}_k(t), (\hat{f}_k^H(t))$	transform of a two-component vector field (transform of a particular field)
r^k	second component of $\mathbf{Z}^{*k}$
t	time
t_1	rise time of a ramp
$T, T(x,t)$	temperature
$U^k, U^k(x)$	eigenfunction of a standard diffusion problem
v	wave velocity
V^k	first component of $\mathbf{Z}^{*k}$
x	abscissa
$\mathbf{Z}^k$	complex vector field

Greek symbols

Δ	difference
$\delta(\cdot)$	Dirac's function
φ, $\varphi(x,t)$, $\psi(x,t)$	flux density
λ	thermal conductivity
μ_k^2	eigenvalue (diffusion problem)
$\theta(x,t)$	temperature
τ	Cattaneo Vernotte time constant
τ'_D	diffusion time ($\tau'_D = e'^2/a'$)
Ω	angular frequency

Subscripts and superscripts

$'$	dimensioned value
$\wedge$	new finite integral transform
$\sim$	standard finite integral transform
$*$	adjoint problem
H	boundary-homogeneous problem
I	initial value
k	eigenelement number
ref	reference value or scaling factor
1, 2	layer number (Clausius problem)

conditions act upon the results, possible deficiencies are not easily interpreted. Recent [6–8], or less recent [9] articles show the influence of such conditions, and *interface* constitutive laws [1] play as decisive a role as *internal* constitutive laws. The weak number of available experiments and the difficulty in attaining a pure problem prompt the use of other independent theoretical models in the testing of an internal continuous law. Transient molecular dynamics (M-D) simulations [10–12] suits this testing. These simulations are not within the framework of a continuous medium; furthermore, since initial and boundary conditions are achieved by controlling the motion of atoms, and since only one medium may be considered in the numerical experiments, questions about the interface constitutive law disappear in a comparison with a continuous model. The problem is thus, in principle, extremely pure and a comparative test of the used internal constitutive law is indeed meaningful.

In the second part of the paper, we use the results of Volz's M-D simulations [10] in a comparison with the analytical solution of the hyperbolic conduction problem obtained with the method introduced in [1]. As is shown below, the method brings a new, but yet incomplete insight into the C–V model.

2. Validation of the new method [1]

We chose a homogeneous medium because we can then apply a standard method of separation of variables [13]. A comparison of the new method with a similar but standard one is thus possible. Moreover, we consider a 1-D problem; in which case we may obtain with a great accuracy as many eigenvalues as we wish, and can thus avoid truncation errors when expanding the solution.

The chosen problem clearly illustrates the differences between the methods; in a standard context—where the problem is reduced to the hyperbolic equation—it is necessary to choose which of the thermal variables should be eliminated. We use a temperature formulation, and thus compare the results for the temperature field only. In view of our previous comments, the treated problem retains an academic character.

2.1. The setting

We consider a film with constant thermophysical properties. This film, which has been kept a long time at a constant temperature, is submitted, in a first stage, to a transient flux ramp on its left-hand side. Then, after a rising time t_1, this flux is maintained at the value it has reached at that time. The right hand side of the film keeps the initial constant temperature value over the entire duration of the simulation.

When the thickness of the film and the diffusion time are chosen as scaling factors for space and time variables, respectively, temperature and flux density inside the film are governed by the following system of non-dimensional equations:

$$\begin{cases} \dfrac{\partial T}{\partial t}+\dfrac{\partial \varphi}{\partial x}=0 \\ \dfrac{\partial \varphi}{\partial t}+\dfrac{1}{\tau}\dfrac{\partial T}{\partial x}+\dfrac{\varphi}{\tau}=0 \end{cases} \qquad 0<x<1,\ \ 0<t, \tag{1}$$

where the normalizing flux density, φ'_{ref}, is the constant incoming flux density when $t_1 < t$ and the normalizing temperature is $e'\varphi'_{\mathrm{ref}}/\lambda'$.

The boundary conditions read as:

$$\text{For } x=0: \quad \begin{cases} \varphi = t/t_1 & \text{if } 0<t\leqslant t_1, \\ \varphi = 1 & \text{if } t_1<t. \end{cases} \tag{2a}$$

$$\text{For } x=1: \quad T=0. \tag{2b}$$

The initial conditions are

$$T(x,0)=0 \quad \text{and} \quad \varphi(x,0)=0 \qquad 0\leqslant x\leqslant 1. \tag{3}$$

2.2. Implementing both methods of solution [2]

We merely recall the various steps. More details about the solution are given in Appendices A (new method) and B (standard method).

The first step consists in splitting up the solution into the sum of a quasi-steady field and a boundary-homogeneous field. When applying the new method, the quasi-steady field is obtained upon considering system (1) for time-independent fields; in the associated boundary conditions (2), the time variable becomes a dummy parameter. When applying standard methods, the flux density must be eliminated, not only within the system (1), but also from the boundary condition (2a), so as to obtain a well-posed problem. This is a first difference between the two methods of solution. It is usual to assume that the constitutive law is valid on the boundary; we have used that hypothesis in Appendix B.

In a second step, the eigenvalue problem is solved. Usually, this step is more involved when implementing the new method because the eigenvalues, which were real-valued when using standard methods, become complex-valued. But, when considering a homogeneous medium, the eigenvalues of the latter are obtained from the eigenvalues of the former as the roots of a second degree polynomial (cf. Appendix A).

The third step is devoted to the computation of the time coefficients of the expansion of the solution of the boundary-homogeneous problem. This computation makes use of the FITs. In the new method, the transform reads as [1]

$$\hat{p}_k(t)=\frac{1}{\langle \mathbf{Z}^k, \mathbf{Z}^{*k}\rangle}\int_0^1 (\theta(x,t)\overline{V}^k(x)+\tau\psi(x,t)\overline{r}^k(x))\,\mathrm{d}x, \tag{4}$$

where Z^k(resp. $\mathbf{Z}^{*k}$) is a vector eigenfunction of the eigenvalue problem (resp., of the adjoint eigenvalue problem), $\theta(x,t)$ and $\psi(x,t)$ are two fields which are defined on the domain under investigation, and $V^k(x)$ and $r^k(x)$ are the two components of $\mathbf{Z}^{*k}$.

In the standard method, the transform reads as

$$\tilde{a}_k(t)=\frac{1}{(U^k,U^k)}\int_0^1 \theta(x,t)U^k(x)\,\mathrm{d}x, \tag{5}$$

where $U^k(x)$ is an eigenfunction of the standard diffusion eigenvalue problem (cf. Appendix B).

When applied to the equations which govern the homogeneous-boundary problem, the FIT (4), (resp., (5)) leads to a first order differential initial-value problem (resp., to a second order initial-value problem).

Upon completion of the previous steps, the final step consists in building an expansion for the solution. When using the FIT (4), the temperature field reads as

$$T(x,t)=\frac{t}{t_1}(1-x)+\sum_k(\hat{p}^{\mathrm{H}}_{k1}(t)+\hat{p}^{\mathrm{H}}_{k2}(t))\cos\mu_k x \quad 0<t\leqslant t_1 \tag{6a}$$

and

$$T(x,t)=1-x+\sum_k(\hat{f}^{\mathrm{H}}_{k1}(t)+\hat{f}^{\mathrm{H}}_{k2}(t))\cos\mu_k x \quad t_1<t. \tag{6b}$$

When using the FIT (5), it reads in turn as

$$T(x,t)=\frac{t}{t_1}(1-x)+\sum_k(\hat{p}^{\mathrm{H}}_{k1}(t)+\hat{p}^{\mathrm{H}}_{k2}(t))\cos\mu_k x + \frac{\tau}{t_1}\left(1-x-2\sum_k\frac{\cos\mu_k x}{\mu_k^2}\right) \quad 0<t\leqslant t_1 \tag{7}$$

and reduces to (6b) during the second stage ($t_1 < t$).

In the writing of the solution with a standard FIT, we have converted the $\tilde{a}_k(t)$ coefficient into its equivalent $\hat{p}_k(t)$ for a more convenient comparison.

2.3. Numerical results

As seen above, a proper comparison of numerical results between both methods is useful only during the first stage of the thermal process. Moreover, upon inspection of Eq. (7), we conclude that the only difference resides in the accuracy of the representation of $(1-x)$ by its expansion:

$$2\sum_k\frac{\cos\mu_k x}{\mu_k^2}.$$

[2] The meaning of "solution" differs in the two methods. In method [1], the solution is a vector whose first component is the temperature and whose second component is the flux density, while, in the standard context, the solution is the temperature field only (the flux-density solution corresponds to a different problem).

Numerical differences will thus be solely due to a truncation effect in the series. Alternate series appear in both formulae and it is well known that these series converge slowly when the time is of the order of a decimal fraction of the unit time. It will thus take—whichever method is used—a very large number of terms for a satisfactory accuracy. Experience shows that the safest criterion in matters of accuracy is the definition of the number zero in early times. As will be seen later, there exists inside the film, at the beginning of the thermal process, an area where the temperature remains zero for small time. If we want this zero temperature to be expressed by a numerical result of order 10^{-6}, it takes about 4000 terms in both expansions, but if we accept a result of order 10^{-4}, 250–300 terms are enough. Whenever accuracy requires many terms, differences between either method are negligible at the scale of a plot. We conclude that both methods give the same results for the temperature field.

We also present, below, some results on the temperature time-derivative field. Since the computed formulae for this field are the same in both methods (as seen by deriving Eqs. (6) and (7)), our goal is merely to obtain useful information on this field. At the numerical level, experience shows that it takes five times more terms in the series expansions to obtain this field with the same accuracy as the temperature field. This difficulty is but a reminder of the limitations of such expansion methods for discontinuous functions.

The transient linear flux which enters the left boundary between times $t = 0$ and $t = t_1$ generates a perturbation whose first front corresponds to the first slope breaking at time $t = 0$, and whose second front corresponds to the slope breaking at time $t = t_1$. This perturbation propagates, while diffusing, at a constant velocity v. In all the presented results, the C–V relaxation time is fixed at $\tau = 0.1$, the corresponding reduced velocity is thus:

$$v = (\tau)^{-1/2} = 3.162.$$

As long as the time is less than $1/v$ (0.3162), the first front has not reached the right-hand side ($x = 1$) of the film and there exists an area where the layer remains in its initial state. After this time, the perturbation reflects on the right boundary; for a period whose duration is equal to the rise time (t_1) of the ramp, the reflected part interferes with the incident part. This period is followed by a purer propagation/diffusion phenomenon of the back-perturbation and so on.

The fronts of the perturbation may be located on the instantaneous temperature profiles of Figs. 1 and 2, thanks to the slope-breaking of the curves. The shorter the rise time of the ramp, the more visible the slope-breaking as observed by comparing the temperature profiles of Fig. 1 (where $t_1 = \tau/2$) to the profiles of Fig. 2 (where $t_1 = 2\tau$). The perturbation, with constant thickness (vt_1) on each figure, is easily identifiable during the first forward traveling period, but, after the first reflection, the interference and the diffusion mask the back-wave. The left-hand side reflection is almost invisible. The temperature profiles quickly become quasi-linear profiles.

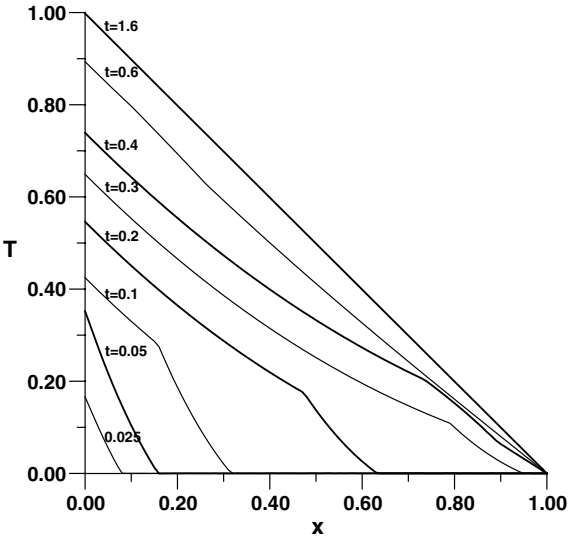

Fig. 1. Instantaneous temperature profiles at different times. Rise-time of the flux ramp $t_1 = 0.05(\tau/2)$.

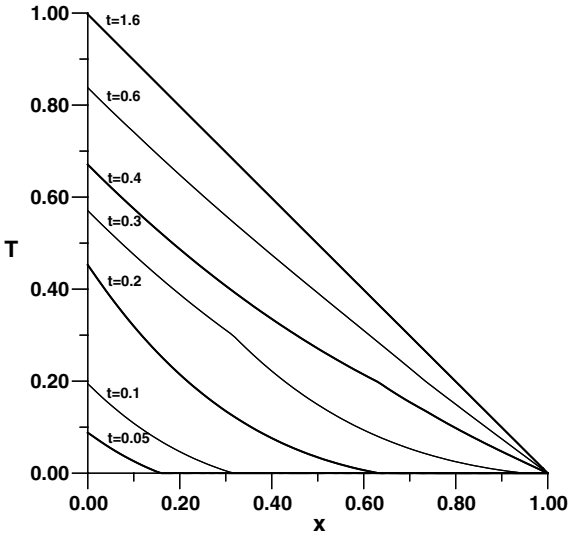

Fig. 2. Instantaneous temperature profiles at different times. Rise-time of the flux ramp $t_1 = 0.2(2\tau)$.

Figs. 3 and 4 show the instantaneous temperature time-derivative profiles for the rise times $t_1 = \tau/10$ and $t_1 = \tau/2$ respectively. The propagation/reflection phenomenon is much more evident on these figures because of the discontinuities which mark the fronts of the per-

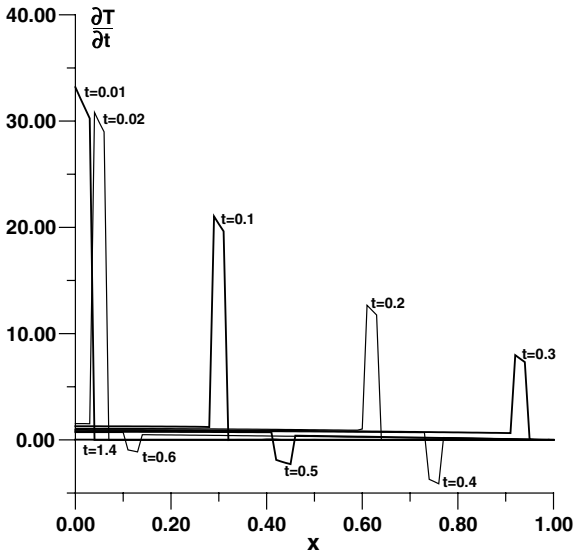

Fig. 3. Instantaneous profiles of temperature time derivative. Rise-time of the flux ramp $t_1 = 0.01(\tau/10)$.

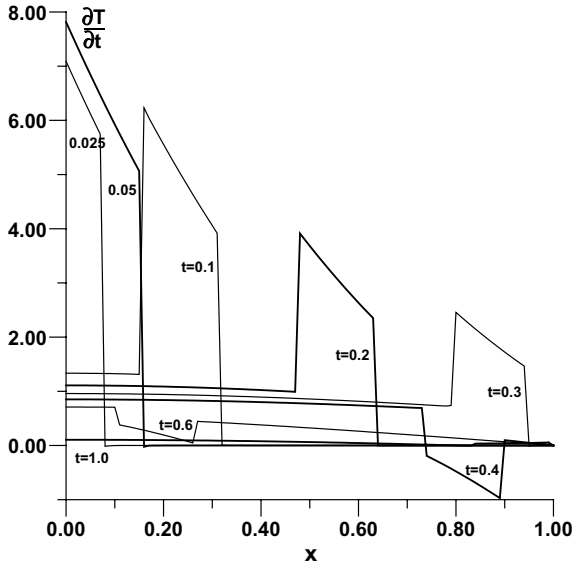

Fig. 4. Instantaneous profiles of temperature time derivative. Rise-time of the flux ramp $t_1 = 0.05(\tau/2)$.

turbation and result in a dented profile. Moreover, the reflection on the right boundary occurs with a change of the sign of $\frac{\partial^2 T}{\partial t\,\partial x}$, which distinctly separates reflected and incident waves. The phenomenon of multiple reflections may be followed for rather long time intervals (up to 10τ), even if, through diffusion, the amplitude of the dents decreases with time.

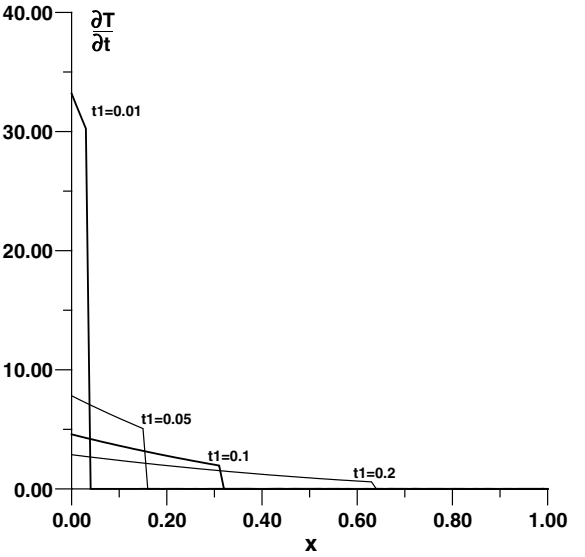

Fig. 5. Instantaneous profiles of temperature time derivative at time t_1.

The shorter the rise time of the ramp, the higher the value of the time derivative on the left-hand side of the film during the first stage of the thermal process. This is evidenced in Fig. 5 where profiles, at the fixed time t_1, for four values of this rise time are gathered together. This is a consequence of the energy balance in the layer, namely

$$\int_0^1 \frac{\partial T}{\partial t}(x,t_1)\,\mathrm{d}x = \varphi(0,t_1) - \varphi(1,t_1).$$

As t_1 is less than $1/v$, no flux crosses the right boundary ($x = 1$); the area under a given temperature time-derivative profile remains constant and equal to the imposed flux on the left boundary. The dent amplitude is thus higher and higher as its thickness (vt_1) becomes smaller and smaller. At the limit $t_1 \to 0$, the $\frac{\partial T}{\partial t}$ profile is a Dirac's delta function, as confirmed by the computation of this limit with the help of the analytical formula.

When considering the response to a flux-step ($t_1 \to 0$), the initial temperature time-derivative field, which is a datum for the methods of solution which are based on the standard hyperbolic equation, must be a Dirac's delta function. Hence a singularity: when the rise time of the ramp is not zero, the initial temperature time-derivative field for a flux ramp problem is zero all over the medium (including boundaries) but not when the rise time vanishes. Frankel et al. [14] mentioned the necessary use of generalized functions when considering step changes in surface temperature. As already explained in the introduction of [1], it is impossible of abruptly varying a function at a given time while maintaining its time derivative to zero at that time. Our observation shows that the initial time-derivative

temperature field must also be a Dirac's function when a *flux*-step is considered on a boundary.

These mathematical intricacies become irrelevant when implementing the new method. The use of physical variables, i.e. temperature and flux density, alleviates the necessity of resorting to generalized functions. Moreover, the standard assumption on the validity of the constitutive law on boundaries—a matter of long-standing debate—is not introduced.

3. Comparison of the results of the Cattaneo Vernotte model with transient molecular dynamics simulations

3.1. A few basics on molecular dynamics simulations

M-D techniques permit the computation of transport properties of materials by applying the laws of mechanics to particles such as molecules and atoms. The solution of the equations of motion of interacting particles, is obtained by numerical integration. In the context of thermal engineering, most studies aim at computing the thermal conductivity of materials [15–17]. Only the final steady state is of importance in such a case and the results are compared to Fourier's law. Few studies investigate transient simulations [10–12], in which case local equilibrium is not reached, at least at the beginning of the simulations. In all cases powerful computers and efficient computation schemes are necessary, because of the smallness of the significant scales. In solids, the space scale is the inter-atomic mean distance and the time scale is the oscillating period of atoms. But the difficulties may be lesser in some crystalline media, firstly because of the periodic structure of the medium, secondly because of the straightforwardness of the expression for the inter-atomic forces.

Volz [10] chooses an argon crystal in which temperatures range from 66 to 250 K, [3] depending on the experiment. This choice saves computation time because of the simple two-body form of the Lennard-Jones potential in the case of argon. The step-by-step solution yields the particle velocities and their displacements. The internal energy of particles in interaction with their neighbors is computed, as is their kinetic energy. Stochastic considerations allow the computation of temperature of particle sets (through the kinetic energy) and of thermal flux densities (through an expression which is derived from the energy balance equation). Initial and boundary conditions are met by controlling the motion of atoms; specific thermostat techniques (acting on the kinetic energy of particle sets) are used for temperature control. These microscopic controls of the simulations allow for a high purity level for the initial and boundary conditions. Even when considering that additional time and space means—which decrease the localization and dynamic sensitivity—are needed in order to reduce the statistical errors, the numerical experiments provide information which is out of reach of true experiments.

3.2. Transient response to a temperature step

3.2.1. Characteristics of the simulation

The argon crystal has been kept at an equilibrium temperature of 67 K which will be chosen as the zero temperature of the thermometric scale. At the beginning, the left side temperature of the simulation cell rises to T_0' (the values 144 and 240 K are used for this controlled given temperature). Periodic boundary conditions are imposed so that the problem is reduced to the study of a layer whose right boundary is adiabatic. The thickness of this layer corresponds to 40 cells of the argon cubic face-centered lattice.

The analytic method does not allow a thermal dependence of parameters. In the following comparison we will choose values of these parameters near their equilibrium value at 144 K (one of the T_0' value). The retained characteristics are shown in Table 1.

In the M-D experiments, the left boundary temperature (T_0') control is performed through a microscopic control of the temperature of a thin film which is adjacent to the studied layer; a thermostat, whose time constant remains less than 0.1 ps in the reported experiments, pilots the temperature rise of the thin film, from the equilibrium temperature to the controlled temperature. The weak value of the time constant, when compared to the C–V time constant (2.35 ps), permits us to view the problem either as a two-stage non-stationary boundary valued problem (with a very short first stage), as was done in Section 2, or as a quasi-temperature step problem. Numerical feasibility and physical considerations motivated our choice of the former.

3.2.2. Computation of the solution of the continuous problem

The left boundary condition is not established instantaneously, this particularity being modeled as a time-varying condition. Thus, during a first stage (duration t_1) the boundary temperature rises linearly from 0 to 1. After that time, the temperature is kept at 1.

Formulae derived from the method [1] are given in Appendix C. Test runs on the computation of the flux showed that, for $x = 0$, and a given small time step δt, the expansion which was based on the temperature step response (cf. Appendix C) converged more slowly than that based on the non-stationary boundary valued problem *when choosing* $t_1 = \delta t$. Moreover, the numerical result, for a given number of terms in the expansions, is always closer to the theoretical result (see below) for the latter case. Such

[3] The medium remains in a solid state up to a temperature of 263 K.

Table 1
Characteristics of the layer

	Thickness (reference space scale)	Diffusion coefficient	Diffusion time scale (reference time scale)	C–V time constant	Thermal wave velocity
SI value	19×10^{-9} (m)	5×10^{-6} (m^2/s)	72×10^{-12} (s)	2.35×10^{-12} (s)	1460 (m/s)
Non-dimensional value	1	1	1	0.03	5.77

considerations prompt the use of formulae corresponding to the two stage problem. In the following results, the first stage duration is always equal to the plotting time step.

We select flux results which are less currently reported in the literature as a first example. Fig. 6 shows the transient flux density which crosses various planes. The motion of a wave which reflects on the adiabatic right face of the layer is clear, but the "visibility" is limited to one bounce only as can be seen by considering the heated left face ($x = 0$) curve. Fig. 7, where four values of the C–V time constants are used, shows that, as the time tends to zero, the flux which crosses the heated left boundary increases as τ decreases. The value of that flux-density jump can be estimated for the temperature step response problem. The temperature inside the layer behaves as a traveling wave whose velocity is v, independently of the right-hand boundary condition (and even in a semi-infinite medium), thus, in the vicinity of the initial time, the temperature may be written as

$$T(x,t) \cong H\left(t - \frac{x}{v}\right) \quad t \to 0_+.$$

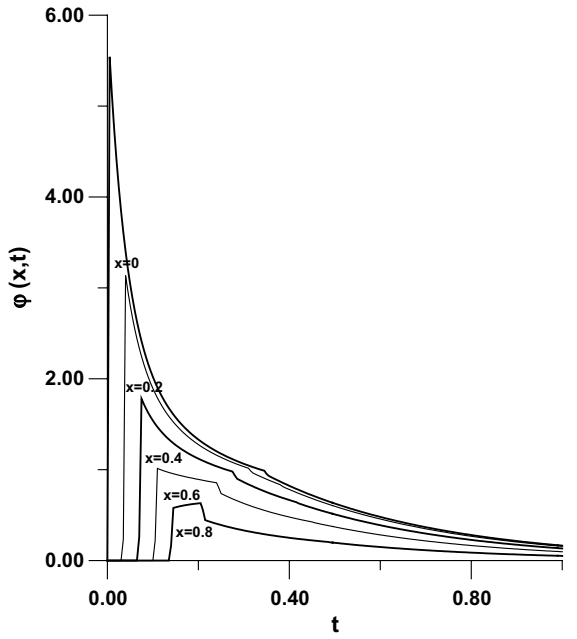

Fig. 6. Time behavior of flux densities crossing different abscissas. Thermal characteristics of Table 1.

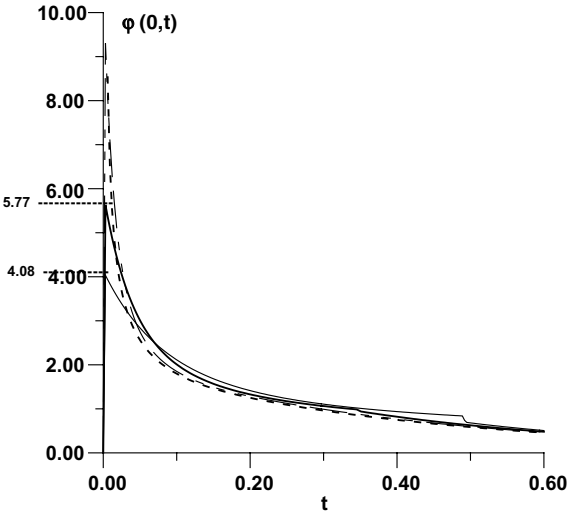

Fig. 7. Incoming flux density ($x = 0$). (- - -) $\tau = 0$ (Fourier model); (–··–··–) $\tau = 0.01$; (—) $\tau = 0.03$ (characteristics of Table 1); (–) $\tau = 0.06$.

The energy balance equation allows an estimation of the flux density which crosses the heated boundary to be made. We obtain

$$\varphi(x,t) \cong \int_0^1 \delta\left(t - \frac{x}{v}\right) \mathrm{d}x \quad t \to 0_+.$$

Its value at $t = 0_+$ is

$$\phi(0,0_+) = v = 1/\sqrt{\tau}.$$

The result is independent of the right limit condition and it demonstrates that the solution of Ref. [18] where the flux density limit is zero at $t = 0_+$, does not satisfy the energy balance equation. Because of the plotting time step in Fig. 7, ($\delta t = 0.003$), the computed value and the above theoretical value (plotted in the figure) are not exactly the same but the discrepancy has been checked to decrease with decreasing time steps.

3.2.3. Comparison with M-D results

A first comparison of our results with M-D results is shown in Fig. 8 for the flux which crosses the left side of the layer. In the original M-D results [10], the flux is divided by the first computed value (i.e. at time $t = 0.06$). This time, which corresponds to the maximum

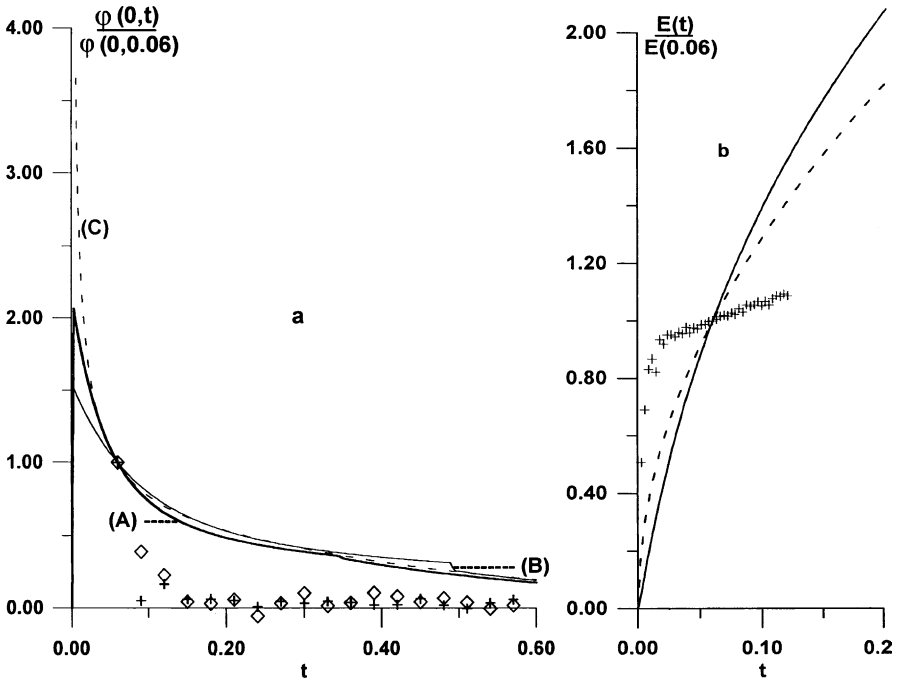

a : Incoming flux density. b : Internal energy.

M-D simulations

◇ $T_0^{'} = 144$ K	
+ $T_0^{'} = 240$ K	+ $T_0^{'} = 240$ K

C-V model

A $\tau = 0.03$ (characteristics of Table I.)	—— $\tau = 0.03$
B $\tau = 0.06$	
C $\tau = 0$ (Fourier model)	----- $\tau = 0$

Fig. 8. Temperature step response.

of the flux curve in Ref. [18] (the used reference in Ref. [10] for a comparison), is unfortunately too high to provide an accurate picture of the early time behavior. Nevertheless, Volz [10] noticed, in his experiments, the high value of the flux immediately after the initial time; he has stressed the inconsistency between this observation and Ref. [18]'s results. But, except for that observation, it appears that, when the parameters of Table 1 are used, the C–V model results (curve (A)) are not compatible with the M-D simulation results. A modification of the τ value will not improve the situation since values greater than 0.03 (curve (B)) or less than 0.03 (curve (C)) yield curves which stay farther apart from the M-D results. The Fourier model results (curve (C)) demonstrate that the origin of the misfit lies in the diffusion time scale value: The equilibrium (0 crossing flux) is reached as early as $t = 0.2$ as far as M-D results are concerned, although, as can be seen in Fig. 6, this equilibrium is not reached at $t = 1$, (it is reached beyond $t = 2$) when the parameters of Table 1 are used.

The integration in space of the local energy balance equation yields:

$$\frac{\mathrm{d}E}{\mathrm{d}t} - \varphi(0,t) = 0. \tag{8}$$

Since the used macroscopic model assumes the standard equilibrium definition of the internal energy, the instantaneous internal energy of the layer is also the space mean temperature of the layer, $\overline{T}(t)$. In M-D simulations, where flux and temperature are computed independently a difference may occur.

Fig. 8b compares C–V results (with parameter values of Table 1) with M-D results for the internal energy. Only the $T_0' = 240$ K case is reported. The high value of

the incoming flux near the beginning of the process is confirmed by considering the slope of the internal energy (owing to Eq. (8), the derivative of E is the incoming flux). But there is no quantitative agreement either with the results of C–V model (solid line) or the results of Fourier model (dotted line).

3.3. Clausius experiment

3.3.1. Characteristics of M-D simulations

Two 10-nm thick layers are separated by an adiabatic surface. They are also insulated from the remaining crystal and brought up to two distinct temperatures ($T_1'^{\mathrm{I}}$, $T_2'^{\mathrm{I}}$) which are then stabilized. Several temperature pairs ranging from 66 to 214 K have been investigated [10,12]. At the initial time the adiabatic partition, which separates the layers, is removed and the time variation of different thermal variables is then followed.

In the following comparison to the C–V model, we will choose the value $\tau = 0.1$ of the C–V reduced time constant; with a diffusion coefficient value of 4.1×10^{-6} m^2/s [12] and a layer thickness, $e' = 10$ nm, the significant diffusion time scale is $=24.4$ ps. The corresponding C–V time constant is thus 2.4 ps. As previously said, non-linearities cannot be taken into account in the used continuous model. The chosen parameter values are only rough estimate values in the considered temperature range.

3.3.2. Solution of the macroscopic continuous problem

The symmetry of the domain implies that the thermal problem which is described in Section 3.3.1 boils down to the study of the temperature step response of each layer where opposite boundaries are adiabatic.

We choose the equilibrium temperature $((T_1'^{\mathrm{I}} + T_2'^{\mathrm{I}})/2)$ as the thermometric origin and we reduce the temperatures by dividing them by $\Delta T'^{\mathrm{I}} = T_2'^{\mathrm{I}} - T_1'^{\mathrm{I}}$. The initial dimensionless temperature is thus $-1/2$ for the first (left) layer and 1/2 for the second (right) layer. The chosen flux density scale is $\varphi'_{\mathrm{ref}} = \lambda' \Delta T'^{\mathrm{I}}/e'$. Only the solution in the right layer is studied; the left-hand layer solution might be immediately computed as

$$\begin{bmatrix} T_1(x_1,t) \\ \varphi_1(x_1,t) \end{bmatrix} = \begin{bmatrix} -T_2(1-x_1,t) \\ \varphi_2(1-x_1,t) \end{bmatrix} \quad 0 < x_1 < 1, \;\; t > 0.$$

The boundary conditions are:

$$T_2(0,t) = 0 \quad \text{and} \quad \varphi_2(1,t) = 0 \qquad t > 0.$$

The solution $T_2(x_2,t)$, $\varphi_2(x_2,t)$ is easily deduced from the detailed solution of Appendix C.

3.3.3. Comparison of results

Fig. 9 permits us to compare the time behavior of the spatial mean temperature $\overline{T_2}(t)$ of the right layer for two configurations of the initial heating. As can be seen here,

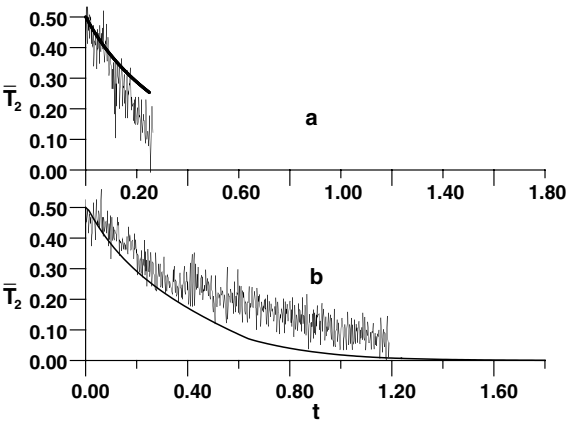

Fig. 9. Clausius experiment: Spatial mean temperature of the right-hand layer. (—) C–V model ($\tau = 0.1$°); (–) M-D model. (a) $T_1'^{\mathrm{I}} = 88.5$ K; $T_2'^{\mathrm{I}} = 136.5$ K and (b) $T_1'^{\mathrm{I}} = 66$ K; $T_2'^{\mathrm{I}} = 103$ K.

the spatial mean computation did not allow the removal of noise in the M-D results. At first glance, the time behaviors are similar for both models, but, the diffusion time scale (24.4 ps) chosen for the C–V model application is ill-suited: it is too high in Fig. 9a but it is too weak in Fig. 9b. This may show a thermal dependence of the parameters for the C–V model. It may be added that a less visible discrepancy between the results of the two models can be noticed. Independently of the noise, Volz [10] indicates the presence of deterministic oscillations in M-D signals. These oscillations—a little more visible in Fig. 9a—are missing on the C–V signals. The only singularity of the latter is at time $t = 0.63$ (Fig. 11b), the time at which the wave created by the contact of the layers at the initial time comes back to the interface between the layers. The deterministic oscillations which appear on M-D signals are probably due to that traveling wave, but our efforts at adapting the τ value so as to recover the fluctuating behavior of the mean temperature have failed. The reason is that, when increasing the τ value, oscillations become visible but, simultaneously, negative temperatures appear in the results as soon as the wave bounces back to the interface for the first time. This appearance of a temperature which oscillates on either side of the long term equilibrium temperature when the C–V time constant increases is a known phenomenon which has been observed in true experimental cryogenic conditions (see [5], p. 860).

Fig. 10 shows the flux density at the interface between the two layers; the M-D results (crosses in Fig. 12) are very noisy. A running average fit with a window width of 11 values (b curve) has thus been added to the original results of Ref. [10]. The local C–V model results appear on the a curve. A significant discrepancy between the two kinds of models is clearly shown: Whereas, according to the M-D computations, the flux density exhibits periodic oscillations with zero mean, the C–V

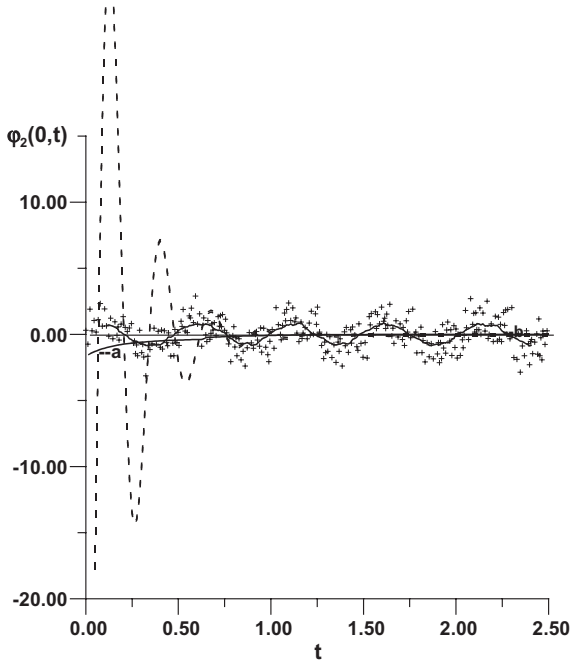

Fig. 10. Clausius experiment: Interface flux density. (a) Local C–V model, (+) M-D model, (b) running average fit of M-D results, (- - -) global C–V model (Ref. [10]).

model results is a flux density that monotonously increases from the value $-1/2\sqrt{\tau}(-1.58)$ to 0. The already noted singularity at time $t = 0.63$ in Fig. 9 is recovered as a flux jump, but the step is barely noticeable at the graph scale. A different C–V model, built on a global thermal balance, has been proposed in Ref. [10]; the equation which governs the interface flux density, $\varphi_2(0,t)$ becomes:

$$\tau\frac{\mathrm{d}\varphi_2}{\mathrm{d}t}+\frac{\Delta T}{2\tau_K}+\varphi_2=0 \quad \text{with } \Delta T=\overline{T}_2(t)-\overline{T}_1(t)=2\overline{T}_2(t).$$

The coefficient $2\tau_K$ is a phenomenological coefficient [10] which may be interpreted as the ratio of a thermal resistance $1/K'$ to the thermal resistance e'/λ' of the layer; furthermore, the ratio τ/τ_K controls the analytical form of solution. A damped sine curve of the form:

$$\varphi_2=-\frac{\exp(-t/2\tau)}{\tau_K}\cos(\Omega t-\alpha) \quad \text{with } \Omega=\frac{\sqrt{\frac{\tau}{\tau_K}-\frac{1}{4}}}{\tau}$$

is obtained (dotted line in Fig. 12). The datum $\alpha = 0$ is proposed in Ref. [10]; the value $\tau_K = 0.018$ is deduced from the same reference, from the previously retained value for $\tau(0.1)$.

Though the global model solution generates oscillations, its solution is still far from the M-D results, notably at time $t = 0_+$ where the flux density of the global model is extremely large (−55). In the same way, at times greater than the diffusion time scale ($t > 1$), the behavior is different; the flux seems oscillating in the M-D results with a significant amplitude to the order of $1/2\sqrt{\tau}$, and this up to $t = 2.0$, although for local and global C–V models this flux is stabilized at 0.

3.4. Discussion

Reported results show a clear disagreement between M-D results and continuous C–V model results. The only positive points, as already mentioned, remains of a qualitative nature:

- In the temperature step response problem the incoming flux is very high at the beginning of the process whichever model is used.
- In the Clausius problem the space mean temperature of each layer has a similar time behavior in both models (ignoring the fluctuations of M-D results).

However, no quantitative agreement is obtained, mainly because of a large difference in long term dynamic properties. Modifying the diffusion time scale—one of the parameters of C–V model—is our first attempt to compel the continuous model to give the same results as the microscopic model.

Fig. 11 shows the obtained results for the temperature step response case when the diffusion time scale is drastically reduced. The fitting is made from M-D incoming flux results (Fig. 11a); we would like to add that the C–V time constant is also modified so as to make the sharp variation of the flux, observed near the first simulation dots (M-D results), coincide with the first bounce of the flux wave (C–V results) on the heated face. The best fits correspond to a diffusion time of 8.64 ps and a C–V time constant of 0.54 ps ($\tau = 0.0625$) when $T'_0 = 144$ K, although the diffusion time is 5.4 ps and the C–V time is 0.86 ps ($\tau = 0.16$) when $T'_0 = 240$ K.

The internal energy, with the same previous adjustments, appears in Fig. 11b. Only the case corresponding to $T'_0 = 240$ K is considered because the other case is not accessible in Ref. [10]; we must remember that it corresponds to the solid line in Fig. 8b. The situation greatly improves, but it may be seen that the results of the two models cannot coincide in both Fig. 11a and b.

Fig. 12 reports Clausius experiment; the diffusion time scale is modified in the same way. Except for oscillations, both models can give the same results when $\tau'_D = 12.2$ ps (Fig. 12a) and when $\tau'_D = 40.7$ ps (Fig. 12b). The corresponding temperature couples of M-D simulations are reported in figure caption. These modifications cannot make the interface flux coincide at all; the corresponding curves are thus not shown.

If we want the Cattaneo Vernotte model to be more than a kind of blackbox, we must think about the

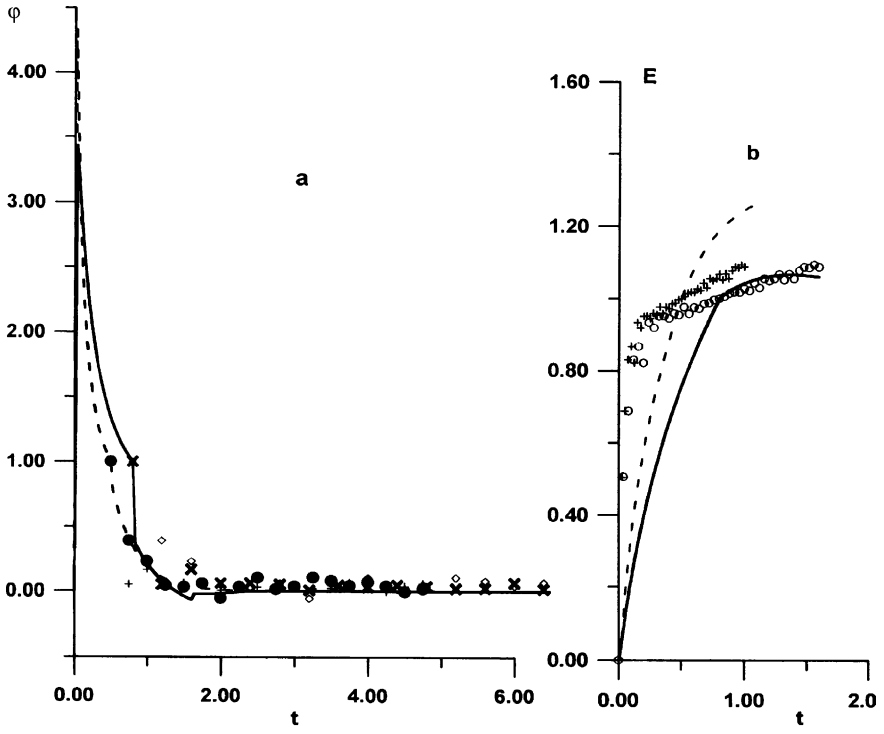

a : Incoming flux density. b : Internal energy.

M-D simulations

$T_0^{'}$ = 144 K	
● with $\tau_D^{'}$ = 8.64 ps as time scale	
◇ with $\tau_D^{'}$ = 5.4 ps as time scale	
$T_0^{'}$ =240 K	$T_0^{'}$ =240 K
+ with $\tau_D^{'}$ = 8.64 ps as time scale	+ with $\tau_D^{'}$ = 8.4 ps as time scale
× with $\tau_D^{'}$ = 5.4 ps as time scale	o with $\tau_D^{'}$ = 5.4 ps as time scale

C-V model

-------- τ= .0625	-------- τ= .0625
———— τ= .16	———— τ= .16

Fig. 11. Temperature step response with diffusion time fits.

physical meaning of these modifications and, possibly, justify them.

Layer thickness is a deciding parameter of the diffusion time. It operates explicitly with a square dependence and may also operate implicitly.

In M-D simulations, boundary conditions are achieved over several atomic planes, so, the thickness of the corresponding layer is not perfectly defined. Owing to the weak size of simulation layers, adding or subtracting few atomic planes to a given layer does induce variations in τ_D'. But these variations remain error terms—say less than 50%—and cannot explain the division by a factor 10 which has been made for the temperature step response case. Moreover the inaccuracy must be the same inside a given experiment since boundary condition achievement is the same. This is not verified at all inside Clausius experiment where the one of the new scale is four times higher than the other. An erroneous thickness value due to boundary condition achievement in M-D simulations is not a dominating cause of erroneous τ_D' values.

Layer thickness may also sometimes modify the thermal conductivity, which acts on the diffusion time. As observed by Lukes et al. [17] in equilibrium M-D

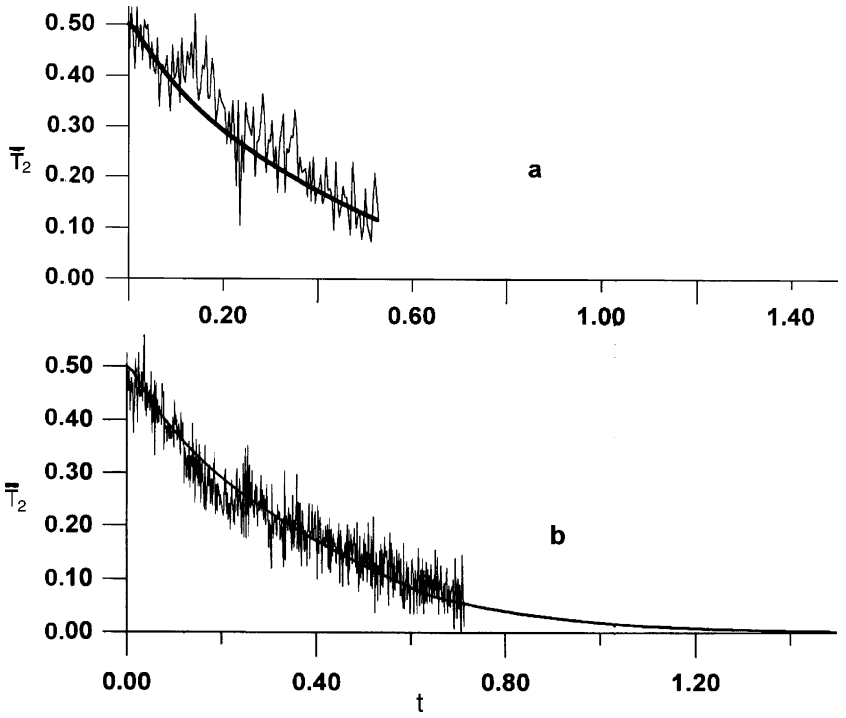

Fig. 12. Clausius experiment: Spatial mean temperature of the right-hand layer with diffusion time fits. (—) C–V model, (–) M-D model. (a) $T_1'^{\mathrm{I}} = 88.5$ K; $T_2'^{\mathrm{I}} = 136.5$ K ($\tau'_{\mathrm{D}} = 12.2$ ps $\tau' = 1.22$ ps) and (b) $T_1'^{\mathrm{I}} = 66$ K; $T_2'^{\mathrm{I}} = 103$ K ($\tau'_{\mathrm{D}} = 40.7$ ps, $\tau' = 4.07$ ps).

simulations, this occurs in adiabatic layers—as opposed to layers with periodic boundary conditions—when the phonon Knudsen number, Kn_{p}, (ratio of the phonon mean free path to the thickness of the layer) is too high. The corresponding lower limit is near $Kn_{\mathrm{p}} = 0.15$ [19]. The present Clausius experiments are concerned with this phenomenon. It may be firstly noticed that the chosen diffusivity value (4.1×10^{-6} m^2/s) has already been reduced in comparison with the value appearing in Table 1. When all assigned to a thickness effect on conductivity, this reduction is not justified in the (a) experiment (Fig. 12a): On the contrary, the conductivity ought to be greater than the bulk conductivity for the new weak value of the diffusion time being explained. In the (b) experiment (Fig. 12b), the reduction is too weak: As seen, a 50% reduction is better and is in accordance with Ref. [17]'s experiments. Unfortunately, since the geometry does not change inside Clausius experiments the previously noticed inconsistency remains.

Variations of conductivity with temperature cannot be rigorously treated since our macroscopic model is linear. Thus, we only examine whether this kind of non-linearity could explain the diffusion time variations. In the considered temperature ranges, conductivity varies as T'^{-1}. Thus, the diffusion time scale should increase—not linearly necessarily—with the mean temperature of the studied layers. The contrary is observed, as much inside the temperature step response problem (the new τ'_{D} value is *lower* for the step 67–240 K than it is for the step 67–144 K), as inside the Clausius experiments.

No explanation based on previously known equilibrium data or results may be called for.

Another troublesome fact is that never is the coincidence between energy and flux results of both models, possible at the same time. These variables are linked together through the energy balance equation (Eq. (8)). The continuous model of course verifies this equation which is the very basis of the computation. M-D results are however less satisfactory.

Considering the temperature step response problem (Fig. 8 or 11), the interval showing a constant value of the slope on Fig. 8b (or Fig. 11b) is not recovered in Fig. 8a (or Fig. 11a) as a constant flux interval. Eq. (8) is badly verified.

The same difficulty arises in Clausius experiment. Integrating Eq. (8) in the right-hand layer leads:

$$E_2(t) - E_2(0) = \int_0^t \varphi_2(0,u)\,\mathrm{d}u. \tag{9}$$

If the equality between $E_2(t)$ and $\overline{T}_2(t)$ is accepted for the microscopic model as for the macroscopic model, M-D results are linked together, in Figs. 9 and 10, in the same way as C–V results. Thus, when the mean temperature of the layer goes from 1/2 to 1/4—which is roughly ob-

served for M-D results in Fig. 9b when the time goes from 0 to 0.4—the left-hand side of Eq. (9) takes the value $1/4 - 1/2 = -1/4$. This is only possible if the flux density (right-hand side of Eq. (9)) exhibits an asymmetry which favors negative values in the interval]0,0.4]. Such an asymmetry does not appear in Fig. 10 for M-D results (b curve).

This difficulty in energy conservation goes beyond the definition of any constitutive law. It prompts several questions:

(i) Is defining macroscopic variables allowed?
(ii) If allowed, are macroscopic variables—notably the internal energy—written correctly?

These questions are not within the scope of this article. However we would point out that Volz [10] tested another model of internal energy where a quadratic flux density term was added to the standard temperature term [20,21]. He concludes that this model is ill-suited to his results. He also mentions the existence of a slight thermo-acoustical coupling in the experiments concerning the temperature step response. This coupling which does not change the look of response curves is responsible on a systematic weak gap—about 10% high—between the internal energy of the layer and its mean temperature. Clausius experiments which are also concerned with the energy conservation difficulty, exhibit no such coupling.

A last point shows how great the difficulty in comparing microscopic to macroscopic results is. The two considered M-D experiments of parts 3.2 and 3.3 differ through the achievement of boundary conditions; more (as long as the flux is concerned) or less large differences in dynamic characteristics correspond to these boundary condition achievements. Considering the macroscopic model, only one basic problem can be associated with both experiments: A layer with one adiabatic face is submitted to a temperature step on the other face. The mutual disposal of two layers of this kind permits both cases to be treated. Thus the basic dynamics, which only depends on the boundary homogeneous problem (see Appendix C), is the same in both problems. One can easily imagine that a simple parameter fit will not be able to lead to the fundamentally different observed behaviors in M-D results; as previously seen, the interface flux shows a quasi-absence of oscillations in the temperature step response experiment but, on the other hand, it shows undamped oscillations up to very large times (2.5 times the diffusion time scale) in Clausius experiment. This last peculiarity appears in other studies. In a certainly different framework where the transient behavior is not studied, Lukes et al. [17] recommend, in thin film [4] M-D simulations, computation times up to 20 times the diffusion time scale if one is to obtain a steady state. In the microscopic model, boundary condition achievement which appears to almost suppress phonons in one case (periodic boundary conditions) exacerbates, on the other hand, their presence in the other case (adiabatic boundaries). This microscopic role of boundaries is not specifically taken into account in macroscopic models. Only a τ increase can give the model the adequate wavy characteristics, but such an increase is not compatible with the used M-D mean temperature results.

One must conclude that, at least as long as the flux is concerned, the C–V model cannot predict the observed transient behavior of adiabatic films in M-D experiments.

[4] Boundary condition achievement is the same as in the present Clausius experiment.

4. Conclusion

The selected test problem (part 2) has shown that the new method of solution of the wave model of conduction gives the same results as a standard method. Moreover, the test brings to light some of the advantages of the new integral transform technique, most notably when the boundaries of the studied domain are not submitted to the same kind of boundary conditions (Dirichlet on part of the boundary and Neumann on the rest of the boundary). The test problem also shows that, when studying the response to a step in boundary conditions, the initial time-derivative field of *temperature* field must be a generalized function, although the step is a *flux* step, in a manner similar to what happens when the step is a temperature step. This remark applies to standard methods of solution but is of no relevance to the new method, since no derivative field is used as data at the initial time in the new method.

Comparison of the Cattaneo Vernotte model to a transient M-D model (part 3) shows a rather tenuous qualitative agreement. The values of thermal parameters must be different from bulk equilibrium values if one strives to obtain a quantitative agreement.

Modifying the diffusion time scale values is the main way for bringing nearer the long term dynamic behavior of the two models; it will be noticed that this long term dynamics is not very different from that of the Fourier model. Nevertheless no objective argument permits the realized modifications to be justified. The C–V model can suit one or the other of the particularly used M-D results, but foreseeing the diffusion time scale values in another given context is not possible at present.

Even when adapting parameters, the results of the two models cannot coincide for both studied variables (internal energy and flux density) at the same time. Two deep reasons seem to cause this anomaly.

Firstly it has been observed that the thermal balance is not satisfactory in M-D results. Since this balance leads to the first partial derivative equation of

the continuous problem, it is of course verified. This explains the incomplete success of parameter fits. Secondly it is seen that the dynamics of M-D results is fairly different from one kind of experiment to the other. This is especially true for the flux. But, in the continuous model, only one basic problem corresponds to both kinds of experiment; the dynamic properties are thus imposed by the same family of eigenvalues. The only adjustment of parameters turns out to be inadequate to completely change these dynamics.

The results of microscopic and macroscopic models are more consistent when considering the response to a temperature step experiment. In the later case the phonon Knudsen number is weaker ($Kn_p \cong 0.3$) than it is in the Clausius experiment ($Kn_p \cong 0.55$). One might deduce that the Cattaneo Vernotte model cannot be used when Kn_p exceeds a value contained within 1/2 and 1/3. Nevertheless, the large dissimilarity between the two M-D experiments, although the phonon Knudsen number hardly doubles, prompts us to consider the upper limit with caution. In fact a special microscopic effect of boundary closeness which appears in isolated films is not modeled in the used continuous model; this phenomenon may affect the purely space scale effect which is expressed in the phonon Knudsen number.

As we have seen the third part of the paper raises more questions that can be solved. These questions concern as much the constitutive law as the energy conservation law, that is to say a basic thermodynamic problem. Whatever the case, based on the previous comparison with transient M-D results, the upper limit of applicability of the Cattaneo Vernotte model would be near a phonon Knudsen number value of 0.5.

Appendix A. Solution of the test problem with the help of the new method

The solution vector $\mathbf{T}$ is split up into two vectors as follows:

$$\mathbf{T} = \mathbf{T}^{S} + \mathbf{T}^{H}.$$

The quasi-stationary field is:

$$\mathbf{T}^{S} = \begin{bmatrix} \frac{s}{t_1}(1-x) \\ \frac{s}{t_1} \end{bmatrix} \text{ if } 0 \leqslant s \leqslant t_1 \quad \text{and}$$

$$\mathbf{T}^{S} = \begin{bmatrix} 1-x \\ 1 \end{bmatrix} \text{ if } t_1 < s.$$

Since there is only one layer in the domain, the transfer matrix of the layer (cf. [1], p. 3315) is the transfer matrix of the film and, for the boundary conditions under consideration, the characteristic equation is obtained by canceling the first coefficient of the transfer matrix. We obtain:

$$\cos\mu = 0 \quad \text{with } \tau\omega^2 - \omega + \mu^2 = 0.$$

The eigenvalues of the problem are the roots of these equations. There are thus two roots ω_{kp} $(p = 1, 2)$ corresponding to each $\mu_k = \pi/2 + k\pi$ $(k = 0, 1, 2\ldots)$ root of the first equation. The vector eigenfunctions of the problem and of the adjoint problem are

$$\mathbf{Z}^{kp} = \begin{bmatrix} \cos\mu_k x \\ \frac{\omega_{kp}}{\mu_k}\sin\mu_k x \end{bmatrix} \quad \mathbf{Z}^{*kp} = \begin{bmatrix} \cos\mu_k x \\ -\frac{\omega_{kp}}{\mu_k}\sin\mu_k x \end{bmatrix}.$$

The temperature in the homogenous boundary value problem expands along a real basis ($\cos\mu_k x$). When the FIT (4) is applied to the homogeneous boundary value problem, the following initial value problems are obtained. During the first stage the problem reads as

$$\frac{\mathrm{d}\hat{p}^{H}_{kp}}{\mathrm{d}t} + \omega_{kp}\hat{p}^{H}_{kp} + \hat{s}_{kp} = 0 \quad p = 1, 2, \ \ 0 < t \leqslant t_1$$

with

$$\hat{p}_{kp}(0) = 0 \quad \text{and}$$

$$\hat{s}_{kp} = \frac{1}{\langle Z^{kp}, Z^{*kp}\rangle}\int_0^1 \left(\frac{(1-x)}{t_1}\cos\mu_k x - \frac{\tau}{t_1}\frac{\omega_{kp}}{\mu_k}\sin\mu_k x\right)\mathrm{d}x,$$

whose solution is

$$\hat{p}^{H}_{kp}(t) = \frac{2(1-\tau\omega_{kp})(1-\mathrm{e}^{-\omega_{kp}t})}{t_1\omega_{kp}(\tau\omega^2_{kp} - \mu^2_k)} \quad p = 1, 2.$$

In a similar manner, the solution during the second stage is

$$\hat{f}^{H}_{kp}(t) = \hat{p}^{H}_{kp}(t_1)\mathrm{e}^{-\omega_{kp}(t-t_1)} \quad p = 1, 2.$$

The first component of the solution vector $\mathbf{T}$ is the temperature field $T(x, t)$ given in Eqs. (6a,b).

Appendix B. Solution of the test problem with the help of a standard method

Eliminating the flux density $\varphi(x, t)$ between the two equations of system (1), the following standard hyperbolic equation is obtained:

$$\tau\frac{\partial^2 T}{\partial t^2} + \frac{\partial T}{\partial t} - \frac{\partial^2 T}{\partial x^2} = 0 \quad 0 < x < 1, \ \ 0 < t.$$

If we assume that the C–V law is valid on boundaries (a standard hypothesis), the boundary conditions are expressed in terms of the temperature field only. The well-posed boundary conditions are thus

$$x = 0 \begin{cases} \frac{\partial T}{\partial x} = -(t+\tau)/t_1 & \text{when } 0 < t \leqslant t_1 \\ \frac{\partial T}{\partial x} = -1 & \text{when } t_1 < t \end{cases}$$

$$x = 1, \ \ T = 0 \quad \text{when } 0 < t.$$

Temperature and time-derivative temperature fields are 0 at the initial time, in the domain as well as on its boundaries.

The same splitting technique as for the new method of solutions yields the following quasi-stationary temperature field:

$$T^{\mathrm{S}}(x,s) = (s+\tau)(1-x)/t_1 \quad 0 < s \leqslant t_1,$$
$$T^{\mathrm{S}}(x) = 1 - x \quad t_1 < s.$$

The eigenvalue problem which must be associated with the standard FIT (5) is the standard eigenvalue problem of diffusion problems, namely,

$$\frac{\mathrm{d}^2 U^k}{\mathrm{d}x^2} + \mu_k^2 U^k = 0 \quad 0 < x < 1,$$
$$\frac{\mathrm{d}U^k}{\mathrm{d}x} = 0 \quad x = 0,$$
$$U^k = 0 \quad x = 1.$$

The eigenvalues μ_k^2 are those of Appendix A. The corresponding eigenfunctions are $U^k = \cos \mu_k x$.

Application of the FIT (5) to the following boundary-homogeneous problems:

$$\tau \frac{\partial^2 T^{\mathrm{H}}}{\partial t^2} + \frac{\partial T^{\mathrm{H}}}{\partial t} - \frac{\partial^2 T^{\mathrm{H}}}{\partial x^2} + \frac{1-x}{t_1} = 0 \quad 0 < t \leqslant t_1,$$
$$\tau \frac{\partial^2 T^{\mathrm{H}}}{\partial t^2} + \frac{\partial T^{\mathrm{H}}}{\partial t} - \frac{\partial^2 T^{\mathrm{H}}}{\partial x^2} = 0 \quad t_1 < t$$

yields the second order initial-value problems which govern the time coefficient $\tilde{a}_k^{\mathrm{H}}$ or $\tilde{b}_k^{\mathrm{H}}$ of the expansion series for $T^{\mathrm{H}}(x,t)$.

In the first stage, the problem reads as

$$\tau \frac{\mathrm{d}^2 \tilde{a}_k^{\mathrm{H}}}{\mathrm{d}t^2} + \frac{\mathrm{d}\tilde{a}_k^{\mathrm{H}}}{\mathrm{d}t} + \mu_k^2 \tilde{a}_k^{\mathrm{H}} + \frac{2}{t_1}\int_0^1 (1-x)U^k(x)\,\mathrm{d}x = 0 \quad 0 < t \leqslant t_1$$

with

$$\tilde{a}_k^{\mathrm{H}}(0) = -\frac{2\tau}{t_1}\int_0^1 (1-x)U^k(x)\,\mathrm{d}x,$$
$$\frac{\mathrm{d}\tilde{a}_k^{\mathrm{H}}}{\mathrm{d}t}(0) = -\frac{2}{t_1}\int_0^1 (1-x)U^k(x)\,\mathrm{d}x.$$

Then,

$$\tilde{a}_k^{\mathrm{H}}(t) = \hat{p}_{k1}^{\mathrm{H}}(t) + \hat{p}_{k2}^{\mathrm{H}}(t) - \frac{2\tau}{t_1 \mu_k^2} \quad 0 < t \leqslant t_1.$$

In the second stage a similar problem arises and its solution is

$$\tilde{b}_k^{\mathrm{H}}(t) = \hat{f}_{k1}^{\mathrm{H}}(t) + \hat{f}_{k2}^{\mathrm{H}}(t) \quad t_1 < t.$$

Note that the initial values $\tilde{b}_k^{\mathrm{H}}(t_1)$ and $\frac{d\tilde{b}_k^{\mathrm{H}}}{dt}(t_1)$ are deduced from $T(x,t_1)$ and $\frac{\partial T}{\partial t}(x,t_1)$ which are in turn computed by running the first stage till t_1.

The complete solution is then constructed; hence Eq. (7) for the first stage and Eq. (6b) for the second stage.

Appendix C. Solution of a two-stage given temperature problem in a slab

The problem reads as

$$\begin{cases} \dfrac{\partial T}{\partial t} + \dfrac{\partial \varphi}{\partial x} = 0 \\ \dfrac{\partial \varphi}{\partial t} + \dfrac{1}{\tau}\dfrac{\partial T}{\partial x} + \dfrac{\varphi}{\tau} = 0 \end{cases} \quad 0 < x < 1, \ 0 < t. \tag{10}$$

The right boundary condition is:

$$\varphi(1,t) = 0 \quad 0 < t.$$

The left boundary condition is:

$$T(0,t) = t/t_1 \quad 0 < t \leqslant t_1,$$
$$T(0,t) = 1 \quad t_1 < t.$$

Temperature and flux density fields are 0 at $t = 0$, in the domain as well as on its boundaries.

The eigenvalues are those obtained in Appendix A. The vector eigenfunctions are

$$\mathbf{Z}^{kp} = \begin{bmatrix} \frac{-\mu_k}{\omega_{kp}} \sin \mu_k x \\ \cos \mu_k x \end{bmatrix} \quad \mathbf{Z}^{*kp} = \begin{bmatrix} \frac{-\mu_k}{\omega_{kp}} \sin \mu_k x \\ -\cos \mu_k x \end{bmatrix}.$$

We set

$$T(x,t) = T^{\mathrm{H}}(x,t) + t/t_1 \quad 0 < t \leqslant t_1,$$
$$T(x,t) = T^{\mathrm{H}}(x,t) + 1 \quad t_1 < t.$$

The boundary-homogeneous problem leads to the following expansion of the temperature field:

$$T^{\mathrm{H}}(x,t) = \sum_k A_k(t) \sin \mu_k x.$$

Setting

$$g_k(u) = \mathrm{e}^{-u/2\tau}\left[\cosh\frac{\sqrt{\Delta_k}}{2\tau}u + \frac{(1-2\tau\mu_k^2)}{\sqrt{\Delta_k}}\sinh\frac{\sqrt{\Delta_k}}{2\tau}u\right],$$

where $\Delta_k = 1 - 4\tau\mu_k^2$, the time-expansion coefficient $A_k(t)$ becomes:

either

$$A_k(t) = \frac{-2}{\mu_k^3 t_1}(1 - g_k(t)) \quad 0 < t \leqslant t_1,$$

or

$$A_k(t) = \frac{-2}{\mu_k^3 t_1}(g_k(t-t_1) - g_k(t)) \quad t_1 < t.$$

The flux density reads as

$$\varphi(x,t)(= \phi^{\mathrm{H}}(x,t)) = \sum_k B_k(t) \cos \mu_k x.$$

Setting

$$h_k(u) = \mathrm{e}^{-u/2\tau}\left[\cosh\frac{\sqrt{\Delta_k}}{2\tau}u + \frac{1}{\sqrt{\Delta_k}}\sinh\frac{\sqrt{\Delta_k}}{2\tau}u\right]$$

the time-expansion coefficient $B_k(t)$ becomes:

either

$$B_k(t) = \frac{2}{\mu_k^2 t_1}(1 - h_k(t)) \quad 0 < t \leqslant t_1$$

or

$$B_k(t) = \frac{2}{\mu_k^2 t_1}(h_k(t - t_1) - h_{\mathrm{k}}(t)) \quad t_1 < t.$$

Remark that, as $t_1 \to 0$, the second stage formulae give the response to a step temperature change problem whose solution is more easily obtained directly. For instance, the flux density expansion reads

$$\varphi(x,t) = \sum_k \frac{4\mathrm{e}^{-t/2\tau}}{\sqrt{\Delta_k}}\sinh\frac{\sqrt{\Delta_k}}{2\tau}t\cos\mu_k x \quad 0 < t.$$

References

[1] P. Duhamel, A new finite integral transform pair for hyperbolic conduction problems in heterogeneous media, Int. J. Heat Mass Transfer 44 (2001) 3307–3320.

[2] C. Cattaneo, Sur une forme de l'équation de la chaleur éliminant le paradoxe d'une propagation instantanée, C.R. Acad. Sci. 247 (1958) 431–433.

[3] P. Vernotte, Les paradoxes de la théorie continue de l'équation de la chaleur, C.R. Acad. Sci. 246 (1958) 3154–3155.

[4] D.Y. Tzou, The generalized lagging response in small-scale and high-rate heating, Int. J. Heat Mass Transfer 38 (1995) 3231–3240.

[5] D.W. Tang, N. Araki, Wavy, wavelike diffusive thermal responses of finite rigid slabs to high-speed heating of laser-pulses, Int. J. Heat Mass Transfer 42 (1999) 855–860.

[6] P. Guillemet, J.-P. Bardon, Conduction de la chaleur aux temps courts: les limites spatio-temporelles des modèles parabolique et hyperbolique, Int. J. Therm. Sci. 39 (2000) 968–982.

[7] W.-B. Lor, H.-S. Chu, Effect of interface thermal resistance on heat transfer in a composite medium using the thermal wave model, Int. J. Heat Mass Transfer 43 (2000) 653–663.

[8] A.E. Kronberg, A.H. Benneker, K.R. Westerterp, Note on wave theory in heat conduction a new boundary condition, Int. J. Heat Mass Transfer 41 (1998) 127–137.

[9] C. Bai, A.S. Lavine, Thermal boundary conditions for hyperbolic heat conduction, Heat Transfer Microscale, ASME, HTD 253 (1993) 37–44.

[10] S. Volz, Transferts de chaleur aux temps ultra-courts par la technique de la dynamique moléculaire, Thèse, Univ. de Poitiers, 1996.

[11] S. Volz, J.-B. Saulnier, M. Lallemand, B. Perrin, P. Depondt, M. Mareschal, Transient Fourier-law deviation by molecular dynamics in solid argon, Phys. Rev. B 54 (1996) 340–347.

[12] S. Volz, M. Lallemand, J.-B. Saulnier, Analyse de la conduction de la chaleur aux temps ultra-courts dans un solide par la thermodynamique irréversible étendue et la dynamique moléculaire, Rev. Géné. Thermique 36 (1997) 826–835.

[13] A. Vedaraz, Heat waves in thermal conduction, PhD dissertation, Polytechnic University, NY, 1994.

[14] J.I. Frankel, B. Vick, M.N. Özisik, General formulation and analysis of hyperbolic heat conduction in composite media, Int. J. Heat Mass Transfer 30 (1987) 1293–1305.

[15] R.D. Mountain, R.A. Mac Donald, Thermal conductivity of crystals: a molecular-dynamics study of heat flow in a two-dimensional crystal, Phys. Rev. B 28 (1983) 3022–3025.

[16] S. Volz, G. Chen, Molecular dynamics simulation of thermal conductivity of silicon nanowires, Appl. Phys. Lett. 75 (1999) 2056–2058.

[17] J.R. Lukes, D.Y. Li, X.-G. Liang, C.-L. Tien, Molecular dynamics study of solid thin-film thermal conductivity, J. Heat Transfer 122 (2000) 536–543.

[18] K.J. Baumeister, T.D. Hamill, Hyperbolic heat conduction equation: a solution for the semi-infinite body problem, J. of Heat Transfer 91 (1969) 543–548.

[19] M.I. Flik, B.I. Choi, K.E. Goodson, Heat transfer regimes in microstructures, J. Heat Transfer 114 (1992) 666–674.

[20] B.D. Coleman, M. Fabrizio, D.R. Owen, On the thermodynamics of second sound in dielectric crystal, Arch. Ration. Mech. An. 80 (1982) 135–158.

[21] C. Bai, A.S. Lavine, On hyperbolic heat conduction and the second law of thermodynamics, J. Heat Transfer 117 (1995) 256–263.